A Novel Harmonic Isolation Method for the Reliable Detection of Rotor Breakages in Induction Motors

Panagiotis A. Panagiotou, *Member, IEEE*, Zihao Song, *Student Member, IEEE*, Jonathan C. Mayo-Maldonado, *Senior Member, IEEE*, Ioannis Arvanitakis, *Member, IEEE*, Gerardo Escobar, *Senior Member, IEEE*, Jose A. Antonino-Daviu, *Senior Member, IEEE*, and Konstantinos N. Gyftakis, *Senior Member, IEEE*

Abstract—**This paper presents a novel methodology for the detection and diagnosis of rotor faults in induction machines using signal estimation. The proposed approach is independent of the motor slip and relies on the isolation of main harmonics rather than on the investigation of signatures with traditional approaches such as the identification of fault-related sidebands. The method is applied on the stator line current capturing the transient nature of fault-related frequencies at the steady state. Thus, it enables a reliable diagnostic strategy by the isolated harmonics and their analysis over time and frequency. The method's effectiveness was explored with electromagnetic simulations of two induction machines of different geometry, manufacture, and power scale. Then, the method was validated experimentally on a 1.1 kW induction motor.**

Index Terms— **harmonic isolation, induction motors, rotor faults.**

I. Introduction

INDUCTION motors are key devices in the modern industry, as they are the main electromechanical energy converters in industrial and production facilities worldwide. This is mainly due to their resilience, reliability, and low cost. Despite that, induction motors are subject to stresses such as thermal and mechanical. At the same time, they frequently operate in environments with adverse conditions that magnify the impact of stresses. Additionally, large motors experience intense electrical stresses due to the stator high voltage. These factors initiate a gradual degradation of motors and their components, resulting in cumulative damage that will progressively lead to a fault condition. The main challenge for diagnostic engineers is to detect faults at incipient levels, to prevent the evolution of the fault into a catastrophic failure.

Rotors of induction motors experience severe stresses both during the transient and the steady-state operation. The impact of frequent start-ups under cold or hot state significantly contributes to the degradation of the rotor cage [1]. Moreover, inherent manufacturing defects such as the porosity of the cage during the casting process create weak points in the rotor structure where hot spots appear, so specific locations of the rotor cage are thermally overstressed [2]. The combination of manufacturing anomalies and stresses during operation may lead to cracks or breakages of the bars and electrical disconnection from the rotor circuit. Rotor faults such as broken bars have been extensively studied over the years [3]. Historically, the Motor Current Signature Analysis (MCSA) was the first method adopted in the field for the detection of this fault. It was considered very reliable until approximately ten years ago, when researchers encountered multiple cases where the method provided false positive or false negative diagnostic outcomes [4]. Therefore, MCSA is still applied but mainly as a first step to identify fault indicators and not as a holistic diagnostic approach. This gap was bridged with the development of other methods exploring several different quantities for fault detection and diagnostics with more sophisticated signal processing techniques [5]-[6].

A false-negative diagnostic case is that of the non-adjacent broken rotor bars [7]. Especially for non-adjacent breakages at half pole pitch distance, the overall magnetic asymmetry can cancel out the signatures in the stator current spectrum making MCSA unreliable [8]. The main solution offered by the research community is to detect the fault during the transient start-up using time-frequency analysis or other advanced signal processing methods [9]-[10]. Although successful, such methods rely on the identification of changing trajectories of fault harmonics over time and cannot always be applied at steady-state. However, there is a vast number of motors in industry that do not undergo frequent start-ups. In these cases, such methods are prone to obscured diagnostic outcomes. A solution for rotor fault detection over the steady state regime of

Corresponding author: Panagiotis A. Panagiotou

P. A. Panagiotou is with the School of Electrical and Electronic Engineering, University of Sheffield, Sheffield, S1 3JD, U.K. (e-mail: p.panagiotou@sheffield.ac.uk).

Z. Song is with the School of Electrical and Electronic Engineering, University of Sheffield, Sheffield, S1 3JD, U.K. (e-mail: zsong15@sheffield.ac.uk).

J. C. Maldonado, with the School of Electronics and Computer Science, University of Southampton, Southampton, SO17 1BJ, U.K. (e-mail: j.mayo@soton.ac.uk).

I. Arvanitakis is with the School of Transport Engineering, Coventry University, Coventry, CV1 2FB, U.K. (e-mail: ac7632@coventry.ac.uk).

G. Escobar is with the School of Engineering & Sciences, Instituto Tecnologico de Monterrey, Monterrey, MX1 11MX, Mexico (e-mail: gescobar@ieee.org).

J. A. Antonino-Daviu is with the Instituto Tecnologico de la Energia, Universitat Politècnica de València, Valencia, VA1 SP1, Spain (e-mail: joanda@die.upv.es).

K. N. Gyftakis is with the Department of Electronic and Electrical Engineering, Technical University of Crete, Chania, CH1 GR1, Greece (email: k.n.gyftakis@ieee.org).

operation was offered by the frequency extraction method at steady state but requires an estimation of the speed and high sampling rate of the monitored current signals [11]-[12].

In this paper, we present a reliable solution for the detection of non-adjacent broken bars during the full-load condition at steady state. The proposed method uses current monitoring and relies on a two-stage signal processing approach enabling frequency isolation. The method has been tested successfully on data from finite element simulations of two induction motors of different sizes and manufacturing characteristics. Finally, this new method has been experimentally validated in the lab, and the experimental results are accurate and complementary to the simulations.

II. Background Theory

A. Rotor Faults in Induction Motors

Rotor fault detection in induction motors has attracted significant research interest with regards to transient detection and extraction of frequency information as intelligent techniques with AI algorithms and neural networks. Regardless of the technique, the characteristic frequencies to detect the fault signature are given by [13]:

$$f_{brb} = [\frac{k}{p}(1-s) \pm s\,]f_s \quad , \tag{1}$$

where $k = 6\nu \pm 1$ …., $\nu \in \mathbb{N}$ …, f_s the fundamental supply frequency, p the number of pole pairs, and s the motor slip. The traditional MCSA-based sideband identification in the vicinity of the fundamental harmonic focuses on the tracking and analysis of the known $(1 \pm 2s\,)f_s$ components due to the developed fault-related speed ripple effect generating such components [1], [2], [8].

The problem of non-adjacent rotor bar breakages forms a special challenge for detection when these occur at the distance of a half-pole pitch and a full-pole pitch. Which is more challenging depends on several factors such as the machine size, geometry, voltage driving the machine, loading conditions, value of slip, manufacture, low-load oscillations, etc., some of which may be beyond the control of the motor end-user or the diagnostician. By way of examples, some combinations of stator slots/rotor bars number introduce more intense speed ripple than others and although the motor is healthy, speed ripple sidebands which are not fault-related may appear in the spectrum; these mislead the diagnostic decision as they appear in the same or similar areas like the components given by (1). Similar is the behaviour of the fault for machines with cooling air-ducts [4], [10]. Other reasons that can lead to erroneous diagnostics are air-voids in the rotor cage (porosity), low values of slip shifting sidebands close to a main harmonic, magnetic anisotropy, and minor delamination or several defective manufacturing features of unknown origin. All these cases and the corresponding physical mechanisms that govern the unpredictable nature of the fault evolution in each case form the framework underlying the rationale of the works described in Section II-B.

B. Digital Signal Processing for Rotor Fault Detection

Several algorithms have been deployed for digital signal processing (DSP) in tandem with condition monitoring and fault detection techniques. Although these approaches come with several novelties and are, to some extent, germane in terms of fault detection during the start-up of the machine by identification of patterns, they are subject to diagnostic inaccuracy. This is because they track the variability of sideband trajectories, which risk being misinterpreted, compromising the diagnostic process. Nonetheless, several research studies in this field have provided compelling fault detection methods with significant contributions, even for some of the challenging cases mentioned in Section II-A.

Initial approaches using time-frequency analysis handled the identification of trajectories by representation with the Wigner-Ville distribution and the Short-time Fourier transform [14]-[15]. These ushered the well-known V-shaped pattern over the transient start-up, which was the fault indication. This trajectory pattern and its behaviour were then put under investigation with other representations such as the wavelet analysis (discrete & continuous, DWT & CWT) [16]-[17], the Hilbert Transform [18], and the multiple signal classification (MUSIC) algorithm [19]. Following this, diagnostic approaches have been investigated using modifications of these methods or their expansion combined with other approaches. Some examples of such novelties were presented in [20] for diagnostics of industrial equipment online using a combination of the STFT and FFT analysis with an embedded system for real-time monitoring, in [21] for eccentricity and rotor faults using Gabor analysis, in [22] for rotor faults and stator faults by the Hilbert-Huang transform, and in [11]-[12] for rotor faults by frequency extraction. Additionally, uncertainties pertaining to frequency fluctuations and their effect in diagnostic competence of traditional methods have been discussed in [23]. In the latter publication, the authors present an efficient approach for the reliable detection of broken rotor bar faults in induction motors by the utilisation of a suppression technique for the sufficient handling of the fundamental frequency component uncertainties caused by frequency fluctuations during the fault detection process.

III. Methodology

A. Frequency isolation algorithm

The main function of the proposed method is the accurate estimation of the fundamental frequency and any higher-order harmonics of a measured signal. $y(t)$. Any such component is a periodical signal, $v(t)$, given by:

$$v(t) = Asin(\omega t + \phi) \quad , \tag{2}$$

where A the amplitude of the signal, ω the angular frequency, and φ the phase angle. Essentially, the signal component expressed by (2) represents the solution of a second-order differential equation of the form:

$$\frac{d^2}{dt^2}v(t) + \omega^2 v(t) = 0 \quad . \tag{3}$$

Using phasors, this solution of (3) in polar form is written as:

$$V = A\angle\phi \quad . \tag{4}$$

The expression given by (4) is a specific odd harmonic that is desired to be isolated, i.e., $\omega = n\omega_m$ with $n = 2l + 1, l \in \mathbb{N}$ and ω_m is the electrical frequency. Considering the state–space formation of (4) and that $v(t)$ is expressed in the α–β frame, it can be written as [24], [26]:

$$v_n(t) = [1 \quad 0]\begin{bmatrix} x_{\alpha,n}(t) \\ x_{\beta,n}(t) \end{bmatrix}, \tag{5}$$

where the subscript n is used to denote the specific harmonic component. After expressing the signal in the α-β frame as in the last equation, then the discrete-time solution of (5) is obtained in the form of a state–space equation [24], [26]:

$$\begin{bmatrix} x_{\alpha,n}[k+1] \\ x_{\beta,n}[k+1] \end{bmatrix} = \begin{bmatrix} \cos(n\omega_m T_s) & -\sin(n\omega_m T_s) \\ \sin(n\omega_m T_s) & \cos(n\omega_m T_s) \end{bmatrix}\begin{bmatrix} x_{\alpha,n}[k] \\ x_{\beta,n}[k] \end{bmatrix}, \tag{6}$$

with T_s being the sampling rate, while the measured signal $y(t)$ can be written as:

$$y(t) = \sum_n v_n(t) = \sum_n x_{\alpha,n}(t) = \\ = x_{\alpha,1}(t) + x_{\alpha,3}(t) + x_{\alpha,5}(t) + \cdots \quad . \tag{7}$$

The algorithm performs an estimation, $[\hat{x}_{\alpha,n}[k] \quad \hat{x}_{\beta,n}[k]]^T$, of the actual components, which must be reliably applied even in the presence of abrupt changes in the signal –i.e., during the transient start-up of the machine or during fractions of the steady-state regime when at fault condition. To accomplish this harmonic isolation, the method presented in [24] & [25] is implemented, which uses the discussed estimation algorithm as a closed-loop scheme for the detection of abrupt transients in power grids. The equations implementing the estimator for each component are given by:

$$\begin{bmatrix} \hat{x}_{\alpha,n}[k+1] \\ \hat{x}_{\beta,n}[k+1] \end{bmatrix} = \begin{bmatrix} \cos(n\omega_m T_s) & -\sin(n\omega_m T_s) \\ \sin(n\omega_m T_s) & \cos(n\omega_m T_s) \end{bmatrix}\begin{bmatrix} \hat{x}_{\alpha,n}[k] \\ \hat{x}_{\beta,n}[k] \end{bmatrix} - \\ - \begin{bmatrix} \varepsilon_n T_s(\hat{y}[k] - y[k]) \\ 0 \end{bmatrix} \quad . \tag{8}$$

Then, the estimated signal is given from:

$$\hat{y} = \hat{x}_{\alpha,1} + \hat{x}_{\alpha,3} + \hat{x}_{\alpha,5} + \cdots \quad , \tag{9}$$

$\hat{x}_{\alpha,n}, \hat{x}_{\beta,n}$ being the estimates of the phasor of the n^{th} harmonic expressed in the α-β frame, $\hat{y}$ is the estimated signal, ω_m the electrical frequency, T_s the sampling rate, and the factors ε_n tuneable adaptation gains with $n = 2l + 1, l \in \mathbb{N}$.

B. Finite Element simulation models

The proposed method is initially implemented with simulations by Finite Element Analysis (FEA) of three different induction motors. The models of each motor and their magnetic flux density distribution are shown in Fig. 1, labelled Motor 1, Motor #2 and Motor #3. Motor #1 and Motor #2 are both 4 kW, 4 poles, 400 V induction motors at 50 Hz, with 36 stator slots and a Δ-connected random-wound distributed stator winding and have 28 rotor bars and 32 rotor bars, respectively. Motor #3 represents a large industrial motor with 1.1 MW output power, 6 poles, 6.6 kV large industrial induction motor at 50 Hz, with 54 stator slots, 70 rotor bars, and a Y-connected concentrated stator winding. Motor #1 and Motor #2 incorporate an aluminium cage, while Motor #3 has a fabricated copper bar cage. The detailed characteristics of these three induction motor simulation models are listed in Table I. Five different FEA models are used for each motor to simulate all required healthy and faulty cases. Using the healthy condition of each induction machine as the basic reference, then four models that refer to the rotor suffering from different bar breakage scenarios are used for each motor, which includes the 1 broken bar, 2 adjacent broken bars, and 2 non-adjacent broken bars being the bar breakage at an angle of half pole pitch and full pole pitch, respectively. By evaluating the diagnosis results using harmonic isolation, the reliability of the proposed technique will be demonstrated on the utilised FEA models. The transient 2-D FEA electromagnetic simulations account for the machine in rotary load-driven motion with a timestep of 0.1 msec, which defines a sampling frequency of 10 kHz for the datasets acquired with simulations. Corresponding to the experimental measurements described after this section, the motors are run at the full-load condition and Table II summarises all the cases per motor as well as the value of slip for each model.

TABLE I
CHARACTERISTICS OF SIMULATED MOTORS

Characteristics	Value		
	Motor #1	Motor #2	Motor #3
Supply frequency	50 Hz	50 Hz	50 Hz
Stator winding	Δ	Δ	Y
Output power	4 kW	4 kW	1.1 MW
Rated voltage	400 V	400 V	6.6 kV
Rated current	10 A	10 A	170 A
Pole pairs	2	2	3
Rated speed	1450 rpm	1450 rpm	990 rpm
Stator slots	36	36	54
Rotor bars	28	32	70

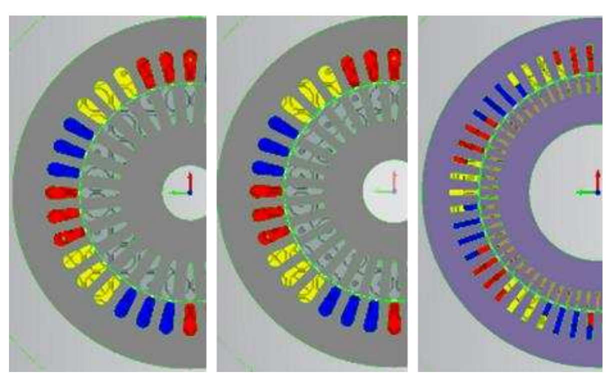

a)

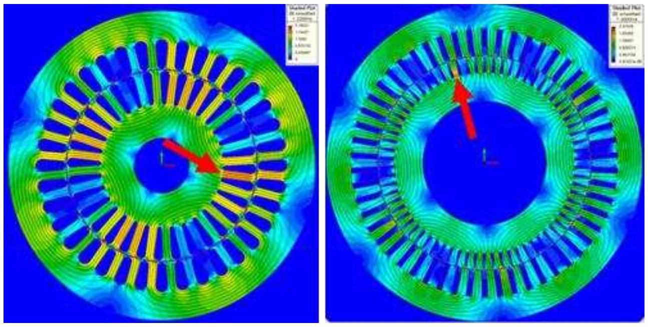

b)

Fig. 1. a) Finite Element Simulation Models: Motor #1 (left), Motor #2 (middle) and Motor #3 (right); b) Magnetic Flux Density Distribution: Motor #1 with 1 broken bar (left), Motor #3 with 1 broken bar (right).

TABLE II
SUMMARY OF MODELS AND VALUES OF SLIP

Cases		Healthy	1 broken bars	2 broken bars adjacent	2 broken bars half-pole	2 broken bars full-pole
Motor#1	**Label**	Healthy	1 BrB	2 BrB	1&4 BrB	1&6 BrB
	Slip	0.0195	0.0204	0.0216	0.0213	0.0213
Motor#2	**Label**	Healthy	1 BrB	2 BrB	1&4 BrB	1&6 BrB
	Slip	0.0174	0.018	0.0189	0.0187	0.0208
Motor#3	**Label**	Healthy	1 BrB	2 BrB	1&6 BrB	1&11 BrB
	Slip	0.0091	0.0094	0.0095	0.0096	0.0094

C. Experimental measurements

The motor used for experiments is a 1.1 kW, 4-pole, 230 V induction motor at 50 Hz, with 36 stator slots, 28 rotor bars, and a Δ-connected distributed winding. Several identical rotors were drilled at different cage locations to emulate the bar breakage scenarios. The cases correspond to four of the five FEA models, thus being the healthy motor and the three cases of rotor breakages (adjacent bars, non-adjacent bars at half-pole pitch, and non-adjacent bars at full-pole pitch angle). Beyond these, two additional cases (non-adjacent bars at positions 1&3 and 1&5) are examined to further verify the accuracy and reliability of the results. The characteristics of the experimental motor are given in Table III, while Fig. 2 illustrates the rotors drilled at the broken bar locations. The test rig utilised for the acquisition of the experimental data has been utilised before in works to the same direction of rotor fault detection in publications such as [11], [19] and [27]-[29], for acquisition of data pertaining to measurements of stator currents and stray flux signals. The experimental measurements were acquired with the machine operating at the full-load condition, corresponding with consistency to the simulation models and conditions. The experimental data were acquired with a sampling frequency of 5 kHz. Table IV provides all the motor cases used for the experimental validation and their slip.

TABLE III
CHARACTERISTICS OF EXPERIMENTAL MOTOR

Characteristics	Value
Supply frequency f_s	50 Hz
Stator winding connection	Δ
Output power	1.1 kW
Rated voltage	230 V
Rated current	4.5 A
Number of pole pairs	2
Rated speed	1450 rpm
Number of stator slots	36
Number of rotor bars	28

a) b) c)

Fig. 2. Rotors of the experimental motor: a) healthy, b) two adjacent broken bars, c) two broken bars at half pole pitch distance.

TABLE IV
SUMMARY OF EXPERIMENTAL MOTORS AND VALUES OF SLIP

Cases	Label	Slip
Healthy	Healthy	0.0173
2 broken bars (adjacent)	2 BrB	0.0186
2 broken bars (non-adjacent)	1&3 BrB	0.0133
2 broken bars (half-pole pitch)	1&4 BrB	0.0126
2 broken bars (non-adjacent)	1&5 BrB	0.0106
2 broken bars (full-pole pitch)	1&6 BrB	0.0127

IV. RESULTS FROM SIMULATIONS

A. Motor #1

The initial step of the proposed method consists of the comparison between the actual and estimated signal by the observer, as depicted in Fig. 3 for the case of a single bar breakage, where the approximation shows that the estimation algorithm has a very good convergence as the steady state signals are almost identical. The next stage is harmonic isolation, where the harmonics of the signal are represented versus time (Fig. 4a) and examined over the frequency domain (Fig. 4b). The latter two steps reveal the changes in the magnitude of each harmonic, enabling the tracking of fault signatures through the examination of the frequency content.

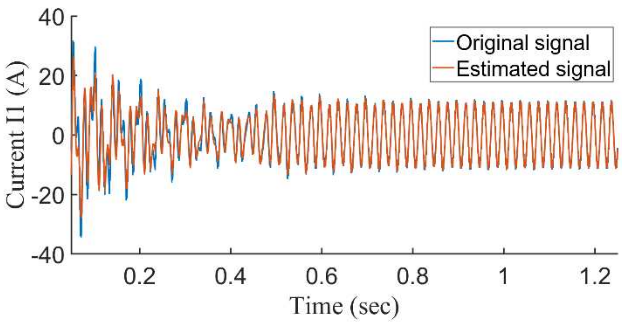

Fig. 3. Representation of the stator current over time: real signal from simulations (blue) and estimated signal using the proposed method (red).

From Fig. 4a (top), the fundamental harmonic carries a mild distortion, which is present in the case of the two adjacent broken bars (2 BrB) and the case of non-adjacent breakage at a full pole pitch. The 5th and 7th harmonic in Fig. 4a (mid and bottom, respectively) have more intense distortions in their magnitude. Nonetheless, except for a slight phase shift, there is no significant difference between the healthy and faulty cases. The frequency content of each isolated signal is shown in Fig. 4b. The sideband at $\pm 2sf$ is present in the spectrum of the fundamental harmonic as given by (2) due to the fault intensifying a speed-ripple effect, which is caused by the distortion in the spatial distribution of the airgap magnetic flux density. This sideband initiates a chain of other fault-related sidebands given by (1). The amplitudes of the two sidebands at $\pm 2sf$ in the fundamental harmonic for every simulated case of Motor #1 are summarised in Table V. The right sideband of the fundamental at $+2sf$ appears at -31.6 dB for the single bar breakage, and at -29.5 dB for two adjacent breakages (2 BrB). For the cases of non-adjacent broken bars, the amplitude of this component is at -40.4 dB for the half pole pitch case (1&4 BrB) and at -36.1 dB for the full pole pitch case (1&6 BrB).

For the 5th harmonic shown in Fig 4b (mid), the discussed sideband gives rise to the $-4sf$ and $-6sf$ components, which are given in Table VI for all cases of Motor #1. An important observation through Fig. 4b (mid) and Table VI for the 5th harmonic is that, although the sidebands at $\pm 2sf$ are weak, the components at $-4sf$ and $-6sf$ are much higher in amplitude. The 5th harmonic components show better diagnostic potential, with the amplitudes of the fault sidebands rising to a level that ranges from -4.8 dB to -9.6 dB. Regarding the 7th harmonic in Fig. 4b (bottom), the $\pm 2sf$ sidebands generate the $-6sf$ and $-8sf$ components. Through Fig. 4b (bottom) and Table VII, a similar conclusion with the 5th harmonic can be drawn for the 7th regarding the lower and upper sidebands, for which the amplitudes rise to a level ranging from -9.8 dB to -4.7 dB.

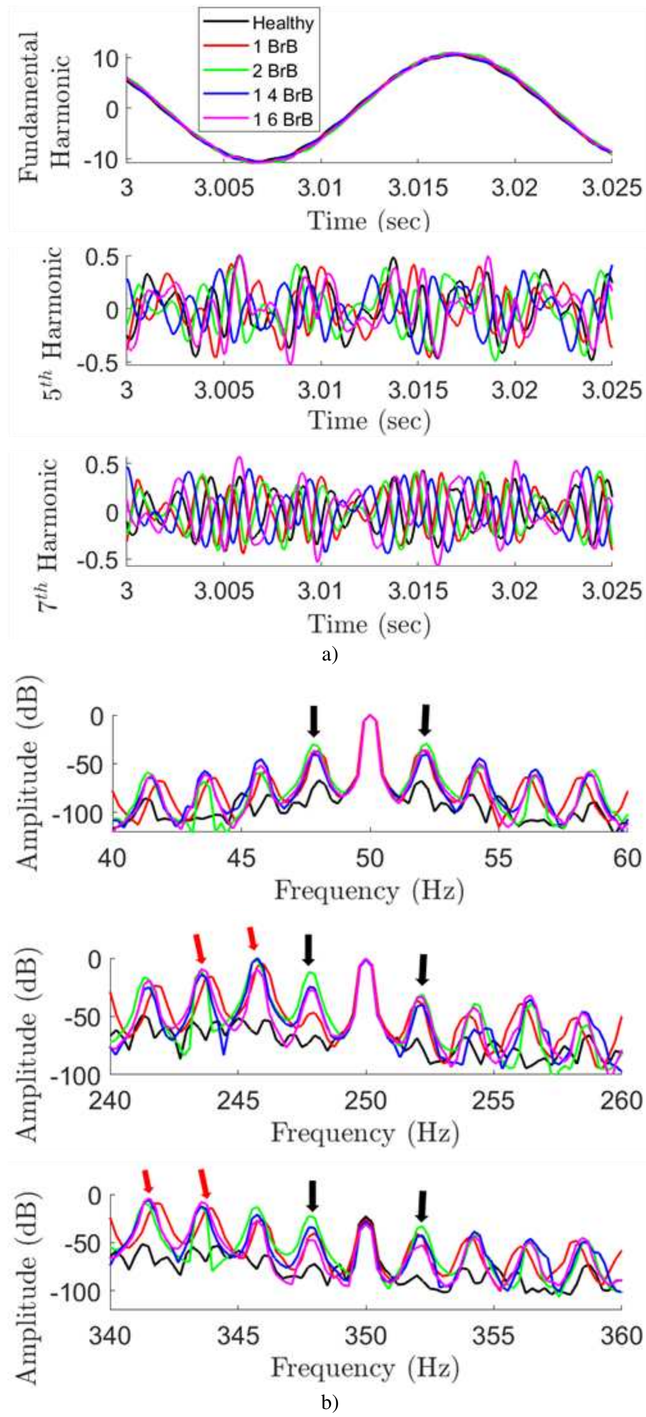

Fig. 4. Diagnostic outcome from Motor #1 by the fundamental harmonic (top), 5th (mid), and 7th harmonic (bottom) of the stator current: a) Frequency isolation b) harmonic content of isolated signals and identification of fault-related frequencies.

TABLE V
AMPLITUDE [dB] OF THE FAULT-RELATED SIDEBANDS IN THE SPECTRUM OF THE ISOLATED FUNDAMENTAL HARMONIC

Motor #1 – Fundamental Harmonic		
Sideband	$+2sfs$	$-2sfs$
Healthy	–	–
1 BrB	-31.6	-36.3
2 BrB	-29.5	-30.1
1&4 BrB	-40.4	-40.4
1&6 BrB	-36.1	-36.9

TABLE VI
AMPLITUDE [DB] OF FAULT-RELATED SIDEBANDS IN THE SPECTRUM OF THE ISOLATED 5TH HARMONIC

Motor #1 – 5th Harmonic				
Sideband	$+2sfs$	$-2sfs$	$-4sfs$	$-6sfs$
Healthy	–	–	–	–
1 BrB	-36.5	-46.7	-4.8	-15.8
2 BrB	-31.3	-11.9	-3.2	-9.5
1&4 BrB	-40	-24.7	-3.2	-13.9
1&6 BrB	-33.4	-27.5	-9.6	-9.5

TABLE VII
AMPLITUDE [dB] OF FAULT-RELATED SIDEBANDS IN THE SPECTRUM OF THE ISOLATED 7TH HARMONIC

Motor #1 – 7th Harmonic				
Sideband	$+2sfs$	$-2sfs$	$-6sfs$	$-8sfs$
Healthy	–	–	–	–
1 BrB	-44.1	-40.3	-14.5	-9.8
2 BrB	-33.1	-22.4	-8.1	-4.7
1&4 BrB	-42.4	-34.1	-12.8	-6.1
1&6 BrB	-52.4	-47.2	-9.1	-6.1

B. Motor #2

The signal distortion of Motor #2 at the fundamental harmonic (top), 5th harmonic (middle) and 7th harmonic (bottom), as shown in Fig. 5a, is similar to that of Motor #1 but with less phase shift. Overall, there is still no notable difference between the healthy and faulty states. Fig. 5b illustrates the fundamental (top), 5th (middle) and 7th (bottom) harmonic content of the isolated stator line current signals for each case of Motor#2. Tables VIII, IX, and X list the fault-related sidebands at the fundamental, 5th and 7th harmonic, respectively.

The magnitudes of the two sidebands at $\pm 2sf_s$ The fundamental harmonics for every simulated instance of Motor #3 are outlined in Table VIII, which corresponds to Fig. 5a (top). The amplitude of the right sideband of the fundamental at $+2sf_s$ is -36.59 dB for the single bar breakage (1 BrB) and -31.92 dB for two adjacent breakages (2 BrB). In non-adjacent broken bars, the amplitude is -38.12 dB for the half-pole pitch scenario (1&4 BrB) and -28.15 dB for the full-pole pitch scenario (1&6 BrB). After observing and comparing Fig. 5b (middle) and Fig. 5b (top), without significant changes in the sidebands at $\pm 2sf_s$, the component amplitudes at $-4sf_s$ and $-6sf_s$ of the 5th harmonic increased significantly. In the relevant components of the 7th harmonic, the same conclusion can be drawn from the observation and comparison of Fig. 5b.

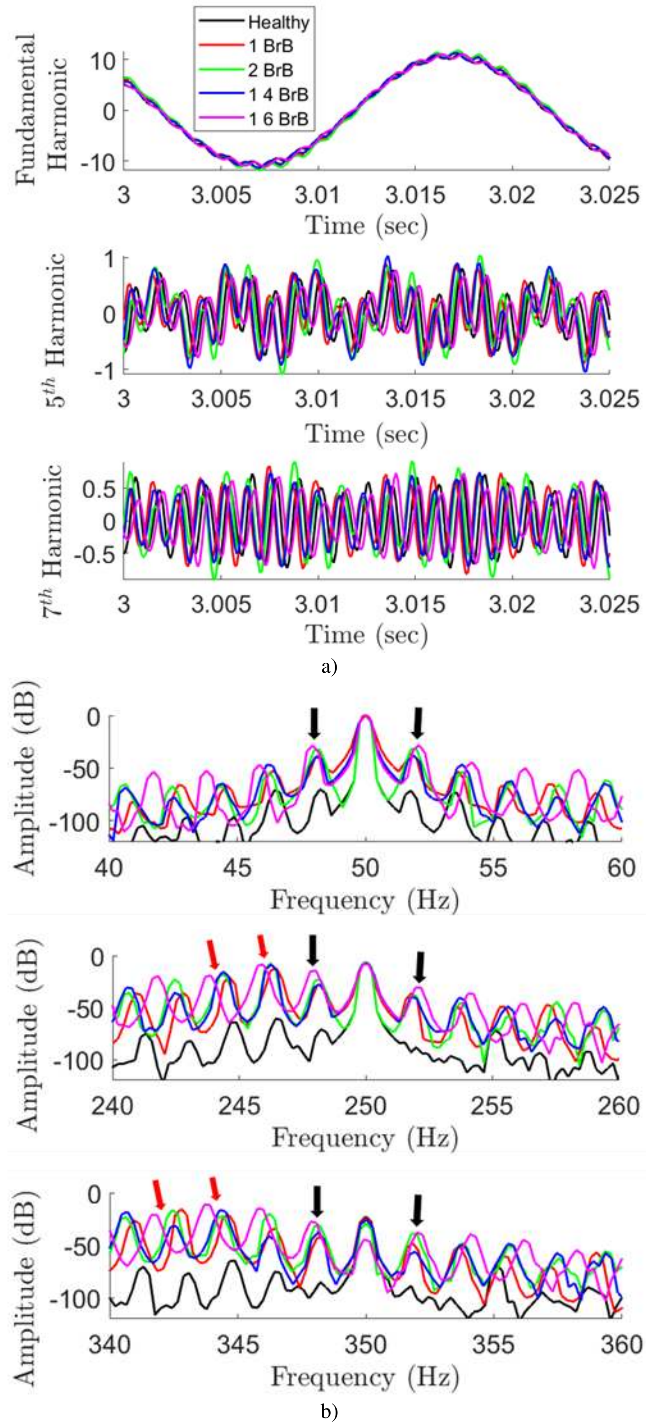

Fig. 5. Diagnostic outcome from Motor #2 by the fundamental harmonic (top), 5th (mid), and 7th harmonic (bottom) of the stator current: a) Frequency isolation b) harmonic content of isolated signals and identification of fault-related frequencies.

TABLE VIII
AMPLITUDE [dB] OF THE FAULT-RELATED SIDEBANDS IN THE SPECTRUM OF THE ISOLATED FUNDAMENTAL HARMONIC

Motor #2 – Fundamental Harmonic		
Sideband	$+2sfs$	$-2sfs$
Healthy	–	–
1 BrB	-36.6	-36.8
2 BrB	-31.9	-32.3
1&4 BrB	-38.1	-39.2
1&6 BrB	-28.2	-28.6

TABLE IX
AMPLITUDE [dB] OF FAULT-RELATED SIDEBANDS IN THE SPECTRUM OF THE ISOLATED 5TH HARMONIC

Motor #2 – 5th Harmonic				
Sideband	$+2sfs$	$-2sfs$	$-4sfs$	$-6sfs$
Healthy	–	–	–	–
1 BrB	-35.9	-27.9	-12	-20.7
2 BrB	-38.4	-22.9	-7.4	-17.9
1&4 BrB	-39.8	-27.4	-8.3	-15.1
1&6 BrB	-30.7	-14.2	-8.3	-18.8

TABLE X
AMPLITUDE [dB] OF FAULT-RELATED SIDEBANDS IN THE SPECTRUM OF THE ISOLATED 7TH HARMONIC

Motor #2 – 7th Harmonic				
Sideband	$+2sfs$	$-2sfs$	$-6sfs$	$-8sfs$
Healthy	–	–	–	–
1 BrB	-47.9	-42.2	-20.6	-15.3
2 BrB	-39.2	-31.1	-22.2	-16.3
1&4 BrB	-55.9	-38	-16.3	-31.9
1&6 BrB	-37.8	-27.4	-11.2	-20.9

C. Motor #3

The results for Motor #3 are presented in Fig. 6. The harmonics of the stator current in Motor #3 have much more intense oscillations over time. These are strongly evident in the cases of two consecutive breakages (2 BrB), and the two cases of non-adjacency (1&6 BrB and 1&11 BrB). The harmonic content of each isolated signal is shown for every case of Motor #3 in Fig. 6b. The main speed-ripple effect components relating with the fault at $\pm 2sf$, are shown for the fundamental harmonic in Table XI. The sidebands of the 5th and 7th harmonic are presented in Table XII and Table XIII, respectively. From Fig. 6b (top), the fundamental does not show any diagnostic potential, as the single bar fault is not adequately captured. However, a very significant observation from Fig. 6b and through Tables XI – XIII, is the capture of the lower and upper sidebands in the content of the isolated signals from the 5th and the 7th harmonic. In these two figures, the proposed approach shows the same diagnostic ability for the two adjacent broken bars, and the two scenarios of non-adjacent breakages. The single bar fault is not captured from the last two columns of Table XII and Table XIII. This is expected for Motor #3 since the fault severity is very low for one bar being broken out of 70 bars in total. However, this fault is reliably captured in the 5th and 7th harmonics using the $-2sf_s$ sideband for identification.

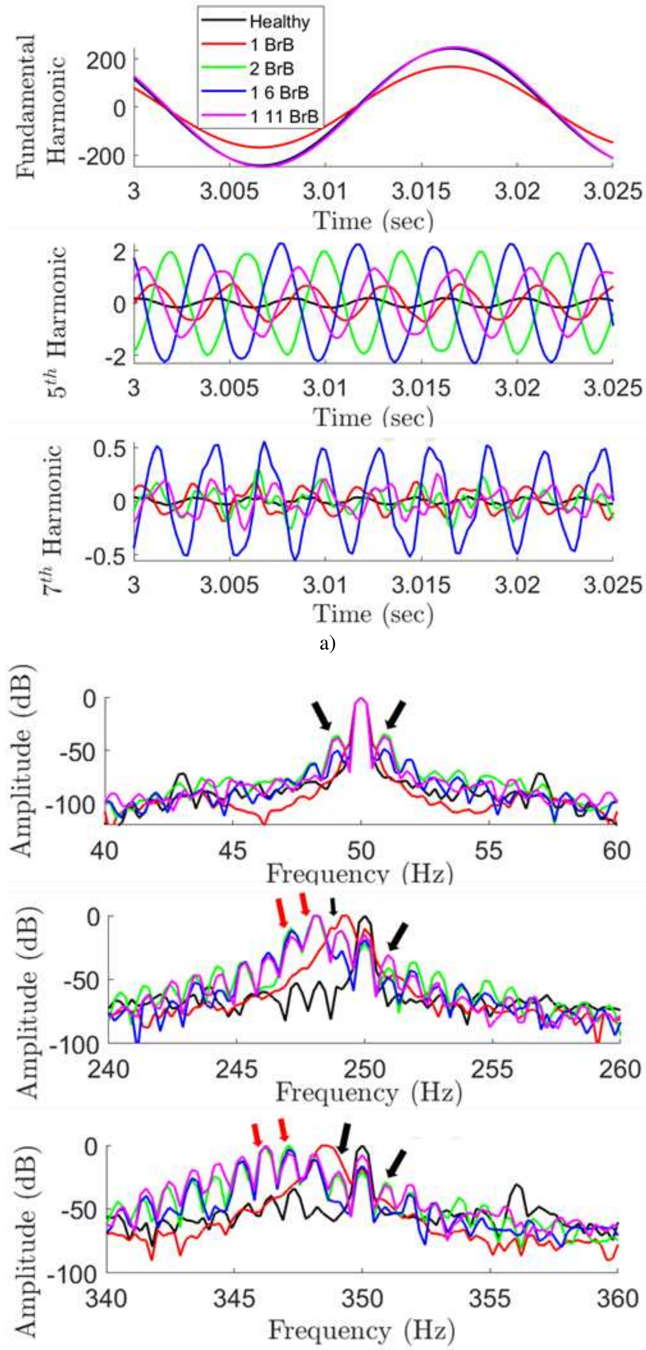

Fig. 6. Diagnostic outcome from Motor #3 by the fundamental harmonic (top), 5th (mid), and 7th harmonic (bottom) of the stator current: a) Frequency isolation b) harmonic content of isolated signals and identification of fault-related frequencies.

TABLE XI
AMPLITUDE [dB] OF THE FAULT-RELATED SIDEBANDS IN THE SPECTRUM OF THE ISOLATED FUNDAMENTAL HARMONIC

Motor #3 – Fundamental Harmonic		
Sideband	$+2sfs$	$-2sfs$
Healthy	–	–
1 BrB	-52.2	-47.4
2 BrB	-34.5	-36
1&4 BrB	-47.6	-50
1&6 BrB	-37.1	-38.3

TABLE XII
AMPLITUDE [dB] OF FAULT-RELATED SIDEBANDS IN THE SPECTRUM OF THE ISOLATED 5TH HARMONIC

Motor #3 – 5th Harmonic				
Sideband	$+2sfs$	$-2sfs$	$-4sfs$	$-6sfs$
Healthy	–	–	–	–
1 BrB	-49	-10.28	-27.5	-40.2
2 BrB	-41.1	-11.6	-0.54	-10.2
1&6 BrB	-48.1	-27.3	-0.51	-11.7
1&11 BrB	-30.8	-11.6	-0.56	-16.3

TABLE XIII
AMPLITUDE [dB] OF FAULT-RELATED SIDEBANDS IN THE SPECTRUM OF THE ISOLATED 7TH HARMONIC

Motor #3 – 7th Harmonic				
Sideband	$+2sfs$	$-2sfs$	$-6sfs$	$-8sfs$
Healthy	–	–	–	–
1 BrB	-42.3	-7.7	-40.9	-49.8
2 BrB	-29.2	-7.3	0.42	-12.7
1&6 BrB	-46.3	-11.7	0.63	-8.8
1&11 BrB	-31.4	-7.7	0.68	-12.1

V. RESULTS FROM EXPERIMENTS

The result of the method on the 1.1 kW experimental motor is shown in Fig. 7. Similarly with Motor #1, the different broken bar conditions in this machine are manifested in the 5th and 7th harmonics, while no significant distortions are present in the fundamental. The fault sidebands are summarised for the fundamental in Table XIV, for the 5th in Table XV, and for the 7th in Table XVI. The sidebands of the fundamental at $\pm 2sf_s$ are relatively weak, whilst the $+2sf_s$ component is not present at all in the 7th harmonic. However, the $-2sf_S$ component shows adequate diagnostic ability both in the 5th and the 7th. From Fig. 7b and through Tables XV–XVI, the lower sidebands in each harmonic are also dominantly present. The $-6sf_s$ sideband of the 5th harmonic is rising in amplitudes ranging from -27.9 dB to -11.7 dB, while the $-8sf_s$ of the 7th ranges from -16.9 dB to -12.9 dB. The most intense amplitude changes are in the two adjacent broken bars, since the localisation of the breakage at consecutive bars creates a larger asymmetry. The results of the harmonic isolation in the experimental motor accurately match the results from the FEA simulations for the several models of Motor #1, Motor #2 and Motor #3.

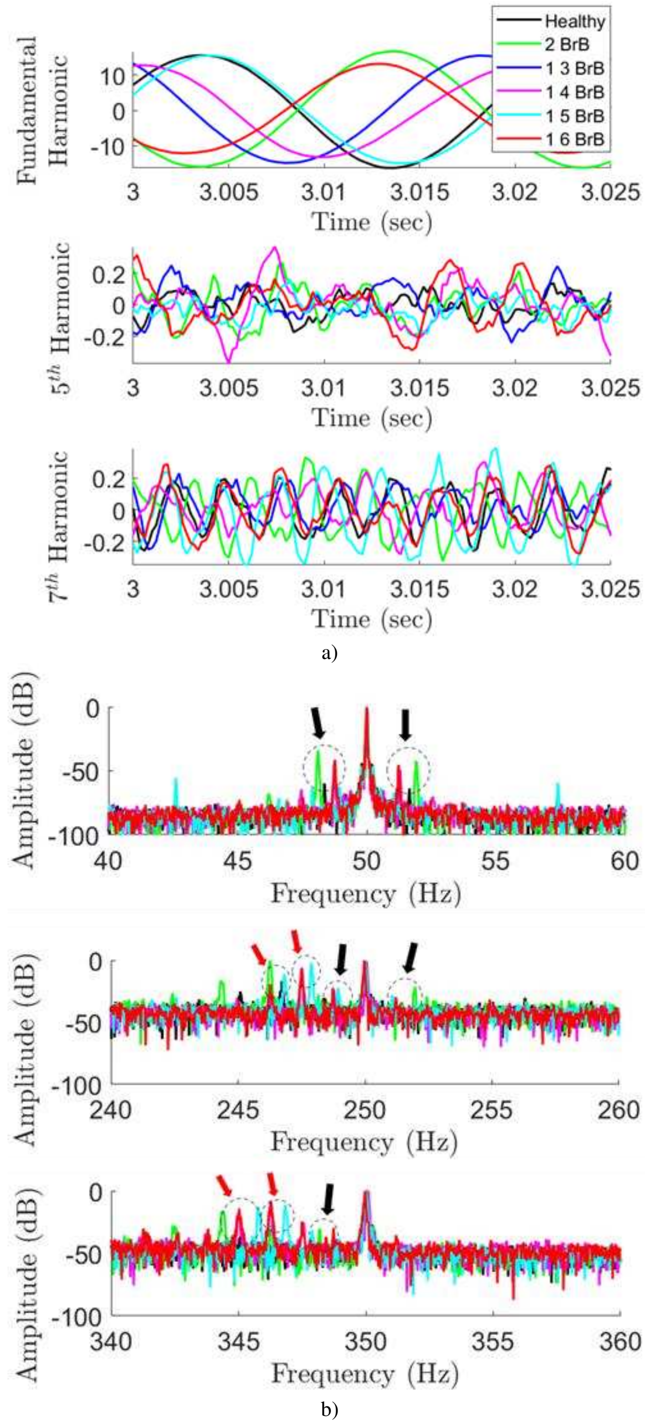

Fig. 7. Diagnostic outcome from experiments by fundamental harmonic (top), 5th (mid), and 7th harmonic (bottom) of the stator current: a) Frequency isolation b) harmonic content of isolated signals and identification of fault-related frequencies.

TABLE XIV
AMPLITUDE [dB] OF THE FAULT-RELATED SIDEBANDS IN THE SPECTRUM OF THE ISOLATED FUNDAMENTAL HARMONIC

Experiment – Fundamental Harmonic		
Sideband	$+2sfs$	$-2sfs$
Healthy	–	–
2 BrB	-42.3	-33.9
1&3 BrB	-49	-44.7
1&4 BrB	-49	-44.7
1&5 BrB	-66.7	-62.3
1&6 BrB	-45.3	-41.4

TABLE XV
AMPLITUDE [dB] OF FAULT-RELATED SIDEBANDS IN THE SPECTRUM OF THE ISOLATED 5^{TH} HARMONIC

Experiment – 5^{th} Harmonic				
Sideband	$+2sfs$	$-2sfs$	$-4sfs$	$-6sfs$
Healthy	–	–	–	–
2 BrB	-21.2	-27.9	0	-16
1&3 BrB	-35.6	-24.3	-6.1	-27.9
1&4 BrB	-35.6	-24.3	-6.1	-27.9
1&5 BrB	-28.5	-22.8	-2.5	-11.7
1&6 BrB	-29.5	-22.5	-7.5	-19.3

TABLE XVI
AMPLITUDE [dB] OF FAULT-RELATED SIDEBANDS IN THE SPECTRUM OF THE ISOLATED 7^{TH} HARMONIC

Experiment – 7^{th} Harmonic				
Sideband	$+2sfs$	$-2sfs$	$-6sfs$	$-8sfs$
Healthy	–	–	–	–
2 BrB	–	-30.3	-27.9	-16.2
1&3 BrB	–	-38.8	-9.4	-16.9
1&4 BrB	–	-38.8	-9.4	-16.9
1&5 BrB	–	-38.1	-10.9	-12.9
1&6 BrB	–	-29.9	-7.8	-14.6

VI. CONCLUSION & FUTURE WORK

This work presented a novel methodology for harmonic isolation using signal estimation in induction motors to reliably track and identify rotor fault-related signatures. The method demonstrated reliable diagnostic ability for the identification of several different broken rotor bar scenarios using the 5^{th} and 7^{th} harmonics. The reliability of the proposed approach was demonstrated on three different induction motors using FEA simulations. Two of these machines were low voltage machines of laboratory scale with an output power of 4 kW where the stator encapsulates a distributed winding and the rotor an aluminium fabricated cage. In contrast, the third motor was an industrial 1 MW induction motor with a concentrated stator winding and rotor manufactured with copper bars. Further, the proposed methodology was also validated with experimental measurements on several scenarios of bar breakage locations using a 1.1 kW induction motor. The proposed method has several benefits, as it is based on a rigorous and efficient estimation algorithm for signal identification in the first stage, which isolates the harmonics of interest to extract the diagnostic information. As such, there is no dependency on the motor slip compared to several existing diagnostic techniques that rely on measurement or estimation of the motor speed. Additionally, this method deploys a diagnostic strategy that is based on the stator main harmonics rather than sidebands, which may or may not appear depending on several factors, some being the motor slip, the spectral leakage, loading abnormalities, and geometry-related factors.

Future work includes the optimisation and fine-tuning of the tuneable adaptive gains in the stage of the estimation algorithm as well as the application of the proposed approach at low loading conditions is an essential future work objective, as such conditions can prove more challenging in terms of fault detection due to increased vibrations at low load. Further, the method's applicability and reliability will be investigated with mechanical measurements, such as the machine torque, and with non-intrusive measurements of electromagnetic quantities, such as stray magnetic flux monitoring.

REFERENCES

[1] W. T. Thomson and I. Culbert, "Current Signature Analysis for Condition Monitoring of Cage Induction Motors", IEEE Press – WILEY, 2017.

[2] M. Jeong, J. Yun, Y. Park, S. B. Lee and K. N. Gyftakis, "Quality Assurance Testing for Screening Defective Aluminum Die-cast Rotors of Squirrel Cage Induction Machines", *IEEE Trans. Ind. Appl*., Vol. 53, No. 3, pp. 2246-2254, 2018.

[3] P. Zhang, Y. Du, T. G. Habetler and B. Lu, "A Survey of Condition Monitoring and Protection Methods for Medium-Voltage Induction Motors," *IEEE Trans. Ind. Appl*., vol. 47, no. 1, pp. 34-46, 2011.

[4] S. B. Lee et all, "Condition Monitoring of Industrial Electric Machines: State of the Art and Future Challenges", *IEEE Ind. Elec. Mag*., Vol. 14, No. 4, pp. 158-167, 2020.

[5] V. Fernandez-Cavero, J. Pons-Llinares, O. Duque-Perez and D. Morinigo-Sotelo, "Detection of Broken Rotor Bars in Nonlinear Startups of Inverter-Fed Induction Motors," *IEEE Trans. Ind. Appl*., vol. 57, no. 3, pp. 2559-2568, 2021.

[6] M. Esam El-Dine Atta, D. K. Ibrahim and M. I. Gilany, "Broken Bar Faults Detection Under Induction Motor Starting Conditions Using the Optimized Stockwell Transform and Adaptive Time–Frequency Filter," *IEEE Trans. Instrum. Meas*., vol. 70, pp. 1-10, 2021.

[7] M. E. Iglesias-Martínez, P. Fernández de Córdoba, J. A. Antonino-Daviu and J. A. Conejero, "Detection of Nonadjacent Rotor Faults in Induction Motors via Spectral Subtraction and Autocorrelation of Stray Flux Signals," *IEEE Trans. Ind. Appl*., 55(5), pp. 4585-4594. 2019.

[8] T. J. Sobczyk and W. Maciolek, "Does the component $(1-2s)f0$ in stator currents is sufficient for detection of rotor cage faults?," *5th IEEE International Symposium on Diagnostics for Electric Machines, Power Electronics and Drives*, Vienna, Austria, 2005.

[9] Y. Park, H. Choi, S. B. Lee and K. N. Gyftakis, "Search Coil-Based Detection of Nonadjacent Rotor Bar Damage in Squirrel Cage Induction Motors," *IEEE Trans. Ind. Appl*., 56 (5), 4748-4757, 2020.

[10] M. S. Rafaq, M. Faizan Shaikh, Y. Park and S. B. Lee, "Reliable Airgap Search Coil Based Detection of Induction Motor Rotor Faults Under False Negative Motor Current Signature Analysis Indications," *IEEE Trans. Ind. Inf*., vol. 18, no. 5, pp. 3276-3285, May 2022.

[11] P. A. Panagiotou, I. Arvanitakis, N. Lophitis, J. A. Antonino-Daviu and K. N. Gyftakis, "A New Approach for Broken Rotor Bar Detection in Induction Motors Using Frequency Extraction in Stray Flux Signals", *IEEE Trans. Ind. Appl*., 2019, 55 (4), 3501-3511, 2019.

[12] D. V. Spyropoulos, P. A. Panagiotou, I. Arvanitakis, E. D. Mitronikas, and K. N. Gyftakis, "Extraction of Frequency Information for the Reliable

Screening of Rotor Electrical Faults via Torque Monitoring in Induction Motors", *IEEE Trans. Ind. Appl.*, 57 (6), 5949-5958, 2021.

[13] J. Faiz, V. Ghorbanian, G. Joksimović, "Fault diagnosis of induction motors". *Institution of Engineering and Technology*, pp. 71-167, 2017.

[14] V. Climente-Alarcon, M. Riera-Guasp, J. Antonino-Daviu, J. Roger-Folch, F. Vedreno-Santos, "Diagnosis of rotor asymmetries in wound rotor induction generators operating under varying load conditions via the Wigner-Ville Distribution", *Int. Symposium on Power Electronics, Electrical Drives, Automation & Motion*, pp. 1378-1383, 2012.

[15] G. Georgoulas, V. Climente-Alarcon, L. Dritsas, J. A. Antonino-Daviu, G. Nikolakopoulos, "Start-up analysis methods for diagnosis of rotor asymmetries in induction motors-seeing is believing". *Mediterranean Conference on Control & Automation (MED)*, pp. 372-377, 2016.

[16] R. Kechida, A. Menacer, "DWT wavelet transform for the rotor bars faults detection in induction motor", International Conference on Electric Power & Energy Conversion Systems, pp. 1-5, 2011.

[17] J. Cusido, L. Romeral, A. Garcia, J. A. Rosero, J. A. Ortega, "Fault detection in induction machines by using continuous and discrete wavelet decomposition", *European Conference on Power Electronics and Applications*, pp. 1-8. 2007.

[18] G. A. Jimenez, A. O. Munoz, M. A. Duarte-Mermoud, "Fault detection in induction motors using Hilbert and Wavelet transforms", *Electrical Engineering*, *89*, pp. 205-220, 2007.

[19] D. Morinigo-Sotelo, R. D. J. Romero-Troncoso, P. A. Panagiotou, J. A. Antonino-Daviu, K. N. Gyftakis, "Reliable detection of rotor bars breakage in induction motors via MUSIC and ZSC". *IEEE Transactions on Industry Applications*, 54 (2), pp. 1224-1234, 2017.

[20] A. Ordaz-Moreno, R. J. Romero-Troncoso, J. A. Vite-Frias, J. R. Rivera-Gillen, A. Garcia-Perez, "Automatic online diagnosis algorithm for broken-bar detection on induction motors based on discrete wavelet transform for FPGA implementation", *IEEE Transactions on Industrial Electronics*, 55 (5), pp. 2193-2202, 2008.

[21] M. Riera-Guasp, M. Pineda-Sánchez, J. Pérez-Cruz, R. Puche-Panadero, J. Roger-Folch, J. A. Antonino-Daviu, "Diagnosis of induction motor faults via Gabor analysis of the current in transient regime", *IEEE Transactions on Instrumentation and Measurement*, 61(6), 1583-1596, 2012.

[22] J. A. Antonino-Daviu, M. Riera-Guasp, M. Pineda-Sanchez, R.B. Perez, "A critical comparison between DWT and Hilbert–Huang-based methods for the diagnosis of rotor bar failures in induction machines. *IEEE Transactions on Industry Applications*. 2009;45(5):1794–1803.

[23] D. A. Elvira-Ortiz, D. Morinigo-Sotelo, A. L. Zorita-Lamadrid, R. A. Osornio-Rios, & R. D. J. Romero-Troncoso, (2020). Fundamental frequency suppression for the detection of broken bar in induction motors at low slip and frequency. Applied Sciences, 10(12), 4160.

[24] G. Escobar, D. Puerto-Flores, J.C. Mayo-Maldonado, J.E. Valdez-Resendiz, O.M. Micheloud-Vernackt, "A discrete-time frequency-locked loop for single-phase grid synchronization under harmonic distortion", *IEEE Trans. on Power Electronics*, 35(5), 4647-4657, 2019.

[25] D. S. Pacheco-Cherrez, J.C. Mayo-Maldonado, G. Escobar, J.E. Valdez-Resendiz, D. Guillen, "A Fully Informative Phasor Measurement Unit for Distribution Networks With Harmonic Distortion", *IEEE Access*, 10, 102575-102585, 2022.

[26] P. A. Panagiotou, J. C. Mayo-Maldonado, I. Arvanitakis, G. Escobar, J. A. Antonino-Daviu, K. N. Gyftakis, "A Novel Method for Rotor Fault Diagnostics in Induction Motors using Harmonic Isolation". In 2023 IEEE 14th International Symposium on Diagnostics for Electrical Machines, Power Electronics and Drives (SDEMPED) (pp. 265-271). IEEE. (2023, August).

[27] Antonino-Daviu, J., Quijano-López, A., Climente-Alarcon, V., & Razik, H. (2017, October). Evaluation of the detectability of rotor faults and eccentricities in induction motors via transient analysis of the stray flux. In 2017 IEEE Energy Conversion Congress and Exposition (ECCE) (pp. 3559-3564). IEEE.

[28] Popaleny, P., & Antonino-Daviu, J. (2018, September). Electric motors condition monitoring using currents and vibrations analyses. In 2018 XIII International Conference on Electrical Machines (ICEM) (pp. 1834-1840). IEEE.

[29] Iglesias Martínez, M. E., Fernández de Córdoba, P., Antonino-Daviu, J. A., & Conejero, J. A. (2020). Detection of adjacent and non-adjacent bar breakages in induction motors based on power spectral subtraction and second order statistics of sound signals. Applied Sciences, 10(19), 6641.

Panagiotis A. Panagiotou (M'22) received the 5-year Diploma (B.S. & M.Eng.) from the Department of Electrical and Computer Engineering of the University of Patras, Patras, Greece, in 2015, and the M.Sc. degree in Complex Systems and Network Theory from the Department of Mathematics of the Aristotle University of Thessaloniki, Thessaloniki, Greece, in 2017. He received the Ph.D. degree in fault diagnostics of electrical machines from Coventry University, Coventry, U.K., in 2020.

In 2021, he joined the Department of Electronic and Electrical Engineering of the University of Sheffield, Sheffield, U.K., as a postdoctoral research associate at the Rolls-Royce University Technology Centre for Advanced Electrical Machines of the University of Sheffield. Since 2022, he is a Lecturer in electrical machines with the School of Electrical and Electronic Engineering of the University of Sheffield, Sheffield, U.K. His research interests include condition monitoring, fault detection and diagnostics in electrical machines, signal processing for diagnostics, and technologies for the inspection and repair of electrical machines.

Dr. Panagiotou is a member of the IEEE, a member of the Institution of Engineering and Technology (IET, U.K.) and a Fellow of the Higher Education Academy (FHEA), U.K.

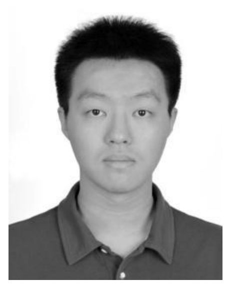

Zihao Song (Student Member, IEEE, '24) received the B.Eng. and the M.Sc. degrees in electronic and electrical engineering from the University of Sheffield, Sheffield, UK, Department of Electronic and Electrical Engineering (EEE), in 2022 and 2023, respectively.

Since 2023, he is a doctoral candidate (PhD student) in diagnostics for electrical machines and drives with the Electrical Machines and Drives research group of the School of Electrical and Electronic Engineering, University of Sheffield, Sheffield, U.K.

His research interests include condition monitoring of electrical machines, fault detection and diagnostics, finite element modelling for fault analysis, and development of fault detection methods.

Jonathan C. Mayo-Maldonado (M'09–SM'22) received the B.Sc. and M.Eng. degrees in electrical engineering from the Instituto Tecnológico de Ciudad Madero, Madero, Mexico, in 2008 and 2010, respectively, and the Ph.D. degree in electrical and electronic engineering from the University of Southampton, Southampton, U.K., in 2015.

From 2015 to 2021, he was a faculty member with the Department of Electrical Engineering, Tecnológico de Monterrey, Monterrey, Mexico. From 2021 to 2025, he was a Lecturer in Electrical Machines and Drives with the School of Electrical and Electronic Engineering of the University of Sheffield, Sheffield, U.K. Since 2025, he is a Lecturer in

Electrical Engineering with the School of Electronics and Computer Science at the University of Southampton, Southampton, U.K.

Dr. Mayo-Maldonado received the Doctoral Control and Automation Dissertation Prize from the Institution of Engineering and Technology in 2015 for his thesis titled “Switched Linear Differential Systems”. His main research interests include system and control theory, condition monitoring in electrification systems, fault detection in electrical machines and drives, power electronics, and smart grid technologies.

Ioannis Arvanitakis received the five-year degree in electrical and computer engineering and the PhD degree from the University of Patras, Patras, Greece, in 2009 and 2017 respectively.

In 2018, he joined Coventry University, Coventry, UK, as an Assistant Lecturer in electrical engineering with the School of Computing, Engineering and Mathematics of Coventry University, Coventry, UK. Since 2021, he has been a Lecturer in electrical engineering with the School of Future Transport Engineering of Coventry University, Coventry, U.K.

His main research interests include navigation, guidance and control, obstacle avoidance algorithms, unmanned ground vehicles, simultaneous localization and mapping algorithms, nonlinear modelling, optimization theory, and digital signal processing.

Gerardo Escobar (Senior Member, IEEE) received the PhD degree in automatic control from the Signals and Systems Laboratory, LSS-SUPELEC, Université de Paris XI, France, in 1999.

From 2008 to 2012, he was a Principal Scientist with the Power Electronics Group, ABB Switzerland Ltd., Zürich, Switzerland. He is currently a Professor-Researcher at the School of Engineering and Sciences, Tecnológico de Monterrey, Nuevo León, Mexico.

His research interests include the modeling, analysis, and control design of power electronic systems, and their applications in renewable energy systems, power quality, grid integration, active filters, batteries, electrical drives, wind power and photovoltaic systems.

Jose A. Antonino-Daviu (Senior Member, IEEE, 2012) received the BS degree in business administration from Universitat de Valencia, Valencia, Spain, in 2012, and the M.S. and Ph.D. degrees in electrical engineering from Universitat Politècnica de València, Valencia, Spain, in 2000 and 2006, respectively. He was with IBM for 2 years, involved in several international projects.

He is currently a Professor with the Department of Electrical Engineering, Universitat de Valencia, where he develops his research work. He was an Invited Professor with Helsinki University of Technology (Finland), in 2005 and 2007, Michigan State University (USA) in 2010, Korea University (South Korea) in 2014, and Université Claude Bernard Lyon 1 (France) in 2015.

He has authored or coauthored more than 300 contributions, including international journals, conferences, and books. Dr. Antonino-Daviu is an Associate Editor for the IEEE Transactions on Industrial Informatics and the IEEE Industrial Electronics Magazine, and he was also IEEE IAS Distinguished Lecturer for 2019-2020. He was General Co-Chair of IEEE SDEMPED 2013 and ICEM 2022. He received the Nagamori Award from Nagamori Foundation in Kyoto, Japan, in 2018, for his contributions in the electric motors transient analysis area. In 2019, he was awarded with the SDEMPED Diagnostic Achievement Award in Toulouse, France.

Konstantinos N. Gyftakis (Senior Member, IEEE) received the five-year Diploma in electrical and computer engineering and the PhD degree in electrical machines condition monitoring and fault diagnosis from the University of Patras, Patras, Greece, in 2010 and 2014, respectively.

Furthermore, he was a Postdoctoral Research Assistant at the Department of Engineering Science, University of Oxford, Oxford, U.K., during 2014-2015. Then, he was a Lecturer from 2015 to 2018 and a Senior Lecturer during 2018–2019 at the School of Computing, Electronics and Mathematics and an Associate at the Research Institute for Future Transport and Cities, Coventry University, Coventry, UK. Between 2019 and 2022 he worked as a Lecturer in Electrical Machines in the School of Engineering and a Member of the Institute for Energy Systems, University of Edinburgh, Edinburgh, UK. He is currently an Associate Professor with the School of Electrical and Computer Engineering, Technical University of Crete, Chania, Greece.

His research interests include fault diagnosis, condition monitoring, degradation, design and electromagnetic analysis of electrical machines. He has authored/co-authored more than 140 papers in international scientific journals and conferences. Dr. Gyftakis serves as Editor for the IEEE Transactions on Energy Conversion and Associate Editor for the IEEE Transactions on Industry Applications.